Molecular graphene under the eye of scattering theory

H. Hammar, P. Berggren, and J. Fransson*
Department of Physics and Astronomy, Uppsala University, Box 516, SE-751 21 Uppsala, Sweden
(Received 30 September 2013; published 12 December 2013)

The recent experimental observations of designer Dirac fermions and topological phases in molecular graphene are addressed theoretically. Using scattering theory, we calculate the electronic structure of finite lattices of scattering centers dual to the honeycomb lattice. In good agreement with experimental observations, we obtain a V-shaped electron density of states around the Fermi energy. By varying the lattice parameter we simulate electron and hole doping of the structure, and by adding and removing scattering centers we simulate, respectively, vacancy and impurity defects. Specifically, for the vacancy defect we verify the emergence of a sharp resonance near the Fermi energy for increasing strength of the scattering potential.

DOI: 10.1103/PhysRevB.88.245418 PACS number(s): 73.20.At, 73.22.Lp, 71.55.−i

I. INTRODUCTION

The interest in Dirac fermions has grown for a wide community after the first synthesis of a monolayer graphene and the subsequent observations of massless fermions.[1–6] As a common feature to a new class of materials that has emerged after the initial breakthrough, the band structure and embedded spin degree of freedom of the Dirac fermions are described by the relativistic Dirac equation.[3,4]

There has been increasing interest in engineered systems that share key properties, including Dirac fermions, with graphene.[7] The hexagonal lattice structure has been shown to be crucial for the formation of Dirac fermions, experimentally realized by, for example, confining photons in hexagonal patterns,[8,9] nanopatterning of ultrahigh-mobility two-dimensional electron gases,[10] scanning probe methods to assemble molecules on metallic surfaces,[11] and trapping ultracold atoms in optical lattices.[12–14] It is important to notice that artificial systems provide alternative routes for studies of topological[15] and quantum spin Hall insulators,[16,17] as well as for novel nontrivial strongly correlated phases.[18]

Although experimental progress within the field of artificially assembled nanostructures has been tremendous, as shown in the above examples, theoretical advances have focused less on aspects of engineered nanostructures. Here, we theoretically study molecular graphene which is constructed by depositing scattering defects in a regular triangular lattice on a metallic surface. Using scattering theory,[19] we calculate the local density of electron states within the engineered lattice structure and find a linear spectrum around the Fermi level, in excellent agreement with experiments.[11] Further, we study the effects of electron and hole doping by modifying the lattice parameter and magnetic field effects by imposing strain to the lattice. Especially, we consider single-defect scattering and simulate both vacancy and impurity defects. For the vacancy defects we verify the emergence of a sharp resonance near the Fermi level for increasing strength of the vacancy scattering potential.

Previous attempts to model molecular, or artificial, graphene have focused on the implementation of infinite lattice structures in two-dimensional electron gases using tight-binding models.[20–22] Here, we instead employ a scattering theoretical approach which allows us to study finite structures of arbitrary size. The flexibility this approach offers has proven invaluable in previous studies of, for example, engineered nanostructures on metallic surfaces[19,23,24] and single defects on topological insulator surfaces[25] and graphene.[26] Our results presented here are hence also an important demonstration of a tool that can be applied more generally for studies of atomic and molecular assemblies embedded in a two-dimensional electron gas.

Local probing techniques are especially promising and useful for building understanding of the interactions in low-dimensional materials and complexes of molecular structures.[27–30] Such techniques have been employed in very different contexts for engineering assembled nanostructures aiming for nanomagnetic memories,[31] spin-based logic gates,[32] and coherent quantum phase measurements.[33]

Scanning tunneling microscopy (STM) is a local probing technique[34] which offers a route for mapping the local electronic structure using the tunneling current flowing between the STM tip and a surface.[35] At low temperatures the tunneling conductance is given by

$$\frac{dI(\mathbf{r},V)}{dV} \propto n_{\rm tip}(\varepsilon_F - eV)N(\mathbf{r},\varepsilon_F), \tag{1}$$

where ε_F is the Fermi level of the system in equilibrium and V is the source-drain voltage applied across the tunneling junction. This expression relates the tunneling (differential) conductance (dI/dV) to the local electronic densities of states (DOS) of the surface (N) and the tip ($n_{\rm tip}$). Typically, the tip electronic density is featureless so that signatures picked up in the tunneling conductance can be attributed to variations in the local surface density of electron states $N(\mathbf{r},\omega)$. Calculating this density is henceforth our primary focus.

II. DEFINING THE SYSTEM

We consider a metallic surface modeled by a two-dimensional electron gas using $\mathscr{H}_0 = \sum_{\mathbf{k}\sigma} \varepsilon_{\mathbf{k}} c^\dagger_{\mathbf{k}\sigma} c_{\mathbf{k}\sigma}$, where $c^\dagger_{\mathbf{k}\sigma}$ ($c_{\mathbf{k}\sigma}$) creates (annihilates) an electron with energy $\varepsilon_{\mathbf{k}}$, momentum $\mathbf{k}$, and spin $\sigma = \uparrow,\downarrow$. Scattering points are inserted at the positions $\mathbf{R}_n$ through the energy $\mathscr{H}_{\rm int} = \sum_n V_n n(\mathbf{R}_n)$, where $n(\mathbf{r}) = \sum_\sigma \int c^\dagger_{\mathbf{k}\sigma} c_{\mathbf{k}'\sigma} e^{-i(\mathbf{k}-\mathbf{k}')\cdot\mathbf{r}} d\mathbf{k} d\mathbf{k}'/(2\pi)^4$ is the electronic charge at the spatial position $\mathbf{r}$. The surface electron density can be calculated through the relation $N(\mathbf{r},\omega) = -{\rm Im}G(\mathbf{r},\mathbf{r};\omega)/\pi$, where $G(\mathbf{r},\mathbf{r}';\omega)$ is the sur-

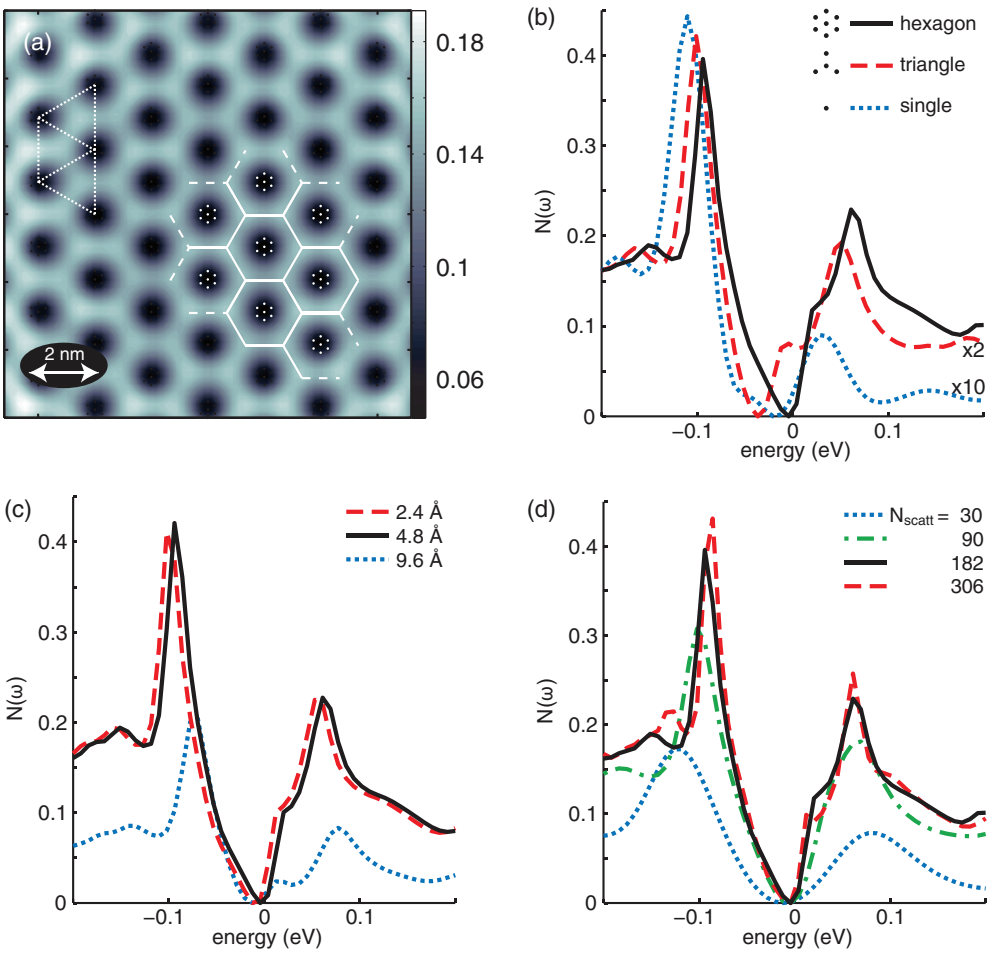

FIG. 1. (Color online) (a) Topograph of a lattice consisting of hexagonal scatterers at an energy of −10 meV. The triangular and hexagonal lattices are added as guides to the eye. (b)–(d) Local DOS as a function of (b) the number of scattering points in each scattering center [seven points (hexagon), four points (triangle), and one point], (c) the diameter of the (hexagonal) scattering centers, and (d) lattice size: 5×6, 9×10, 13×14, and 17×18 (hexagonal) scattering centers. In (a), (b), and (d) we used a diameter of 4.8 Å for the hexagonal scattering centers and lattice parameter $a = 19.2$ Å. For all plots we have used $\varepsilon_{\mathbf{k}} - \varepsilon_F = E_0 + \hbar^2 k^2/2m^*$, with $E_0 \simeq -0.45$ eV for Cu(111), and $m^* = 0.38m$, where m is the free-electron mass.

face Green's function (GF) which describes the local electronic structure. The real-space GF connects to the introduced model through the Fourier transform $G(\mathbf{r},\mathbf{r}';\omega) = \int G_{\mathbf{k}\mathbf{k}'}(\omega) e^{i\mathbf{k}\cdot\mathbf{r} - i\mathbf{k}'\cdot\mathbf{r}'} d\mathbf{k} d\mathbf{k}'/(2\pi)^4$. Here, we have suppressed the spin indices since our system is assumed to be perfectly spin degenerate.

The *dressed* GF G is constructed through a T-matrix expansion (see, for example, Refs. 19 and 36 for more details),

$$G_{\mathbf{k}\mathbf{k}'}(\omega) = \delta(\mathbf{k}-\mathbf{k}')g_{\mathbf{k}}(\omega) + \sum_{mn} g_{\mathbf{k}}(\omega) e^{-i\mathbf{k}\cdot\mathbf{R}_m} \times \mathscr{T}(\mathbf{R}_m,\mathbf{R}_n) e^{i\mathbf{k}'\cdot\mathbf{R}_n} g_{\mathbf{k}'}(\omega), \quad (2a)$$

$$\mathscr{T}(\mathbf{R}_m,\mathbf{R}_n) = t(\mathbf{R}_m,\mathbf{R}_n) V_n, \quad (2b)$$

where $t^{-1}(\mathbf{R}_m,\mathbf{R}_n) = \delta(\mathbf{R}_m - \mathbf{R}_n) - V_m g(\mathbf{R}_m - \mathbf{R}_n)$, $g(\mathbf{r}-\mathbf{r}') = \int g_{\mathbf{k}} e^{i\mathbf{k}\cdot(\mathbf{r}-\mathbf{r}')} d\mathbf{k}/(2\pi)^2$, and the *bare*, or unperturbed, GF $g_{\mathbf{k}} = (\omega - \varepsilon_{\mathbf{k}} + i\delta)^{-1}$, where $\delta > 0$ is infinitesimal. This expansion describes the influence of scattering at the positions $\mathbf{R}_m$ on the electronic structure by providing a correlation between electron creation at $\mathbf{r}'$ and annihilation at $\mathbf{r}$ in the presence of potential scattering.

The scattering potentials at sites $\mathbf{R}_m$ deplete the electron density in a neighborhood around those positions, and this electron density has to be redistributed elsewhere in the structure. This generates a new electronic structure. By distributing the scattering potentials according to a triangular lattice (dotted lines), we construct an electronic density which is distributed as a honeycomb lattice; see Fig. 1(a).

III. Results

A. Lattice conditions

In an experimental setup, the scattering centers would be represented by atomic or molecular entities,[11] which provides a continuous and spatially extended potential landscape. While we have used Dirac pointlike scattering potentials, $V_n = \int V_0 \delta(\mathbf{r} - \mathbf{R}_n) d\mathbf{r}$, in our calculations, spatial extension of the scattering centers can be obtained by inserting several scattering points in cluster formations [see the legend of

Fig. 1(b)]. The electron DOSs resulting from three different types of scattering centers are plotted in Fig. 1(b): single scattering points (dotted line), four points in a triangular form (dashed line), and seven points in a hexagonal form (solid line). The plotted electron DOSs are obtained by spatially averaging around the scattering centers and subtracting the flat background density of the surface states. The plots clearly illustrate how the spatial extension of the scattering centers build up the linear spectrum around the Fermi level (zero-energy point), the Dirac point, and we base our following discussion on the hexagonally shaped scattering centers.

Furthermore, we test the importance of the spatial extension of the scattering centers by varying the diameter of the hexagonally shaped scattering centers, and in Fig. 1(c) we plot the electron DOS for different sizes. The resulting DOSs point towards the fact that scattering centers of about 2–5 Å in diameter are sufficiently large to *not* have a pointlike influence on the electronic density. Scattering centers that are too large (diameter $\gtrsim 9$ Å) tend, on the other hand, to modify the electronic density towards a double-well structure around the Fermi level.

The lattice size has a natural influence on the electron DOS at the center of the lattice [see Fig. 1(d), where we plot the electron DOS as a function of the lattice size]. Distributing scattering centers with a diameter of 4.8 Å in a triangular lattice with lattice parameter $a = 19.2$ Å clearly indicates that the central electron DOS converges towards a linear spectrum around the Fermi level sufficiently well for 100–200 scattering centers arranged in a nearly quadratic form.

B. Lattice functionalization

Changes in the lattice parameter a have the influence of doping the molecular graphene. A smaller (larger) lattice parameter functions as a stronger (weaker) confinement of the electron density, which thereby pushes the spectrum towards higher (lower) energies [see Fig. 2(a)]. In this way one can achieve electron (hole) doping of the system. Apart from the rigid shift, the shape of the spectrum remains nearly unaffected by the changes in the lattice parameter.

The flexibility offered by the scattering theoretical approach is illustrated by the spectrum plotted in Fig. 2(b), showing the electron DOS for a Kekulé textured lattice (see inset). In excellent agreement with the experiments,[11] we reproduce the opening of a finite gap at the Dirac points, as well as the strong peaks appearing on each side.

Imposing strain, or pseudomagnetic field, on molecular graphene has the same effect as in real graphene, namely, breaking the pseudospin symmetry of the Dirac point. Practically, a constant strain field is introduced through displacement of the scattering centers, in polar coordinates (r,θ), using $(u_r,u_\theta) = (qr^2 \sin 3\theta, qr^2 \cos 3\theta)$, where q is a parameter for the strength of the strain.[17]

In Fig. 3(a) we show the spectral density at the center of the lattice for strain conditions corresponding to a magnetic field of 60 T. In agreement with experiments, the strain breaks the pseudospin symmetry of the Dirac point, which becomes visible in the spatial resolution of the spectral density. This results in the formation of an A sublattice with increased density at the Fermi level (bright spots) and a B sublattice with reduced density (dark spots). This is more clearly shown in Fig. 3(b), where we plot the local DOS associated with the respective sublattices. The local DOS shows a well-defined zero-energy state, the zero Landau level, in the bright spots of the A sublattice (solid line). The dark regions of the B sublattice (dashed line) are associated with a reduced electron density, revealing the Landau gap below the Fermi level.

C. Impurity scattering

Next, we consider impurity scattering in molecular graphene. Before we proceed, however, we briefly introduce the salient features predicted for impurity scattering in graphene. It has been shown that simple potential scattering at the position $\mathbf{R}_0$ gives rise to a resonance in the local electron DOS below the Dirac point but within the linear part of the spectrum.[37–39] We discuss the results within a nearest-neighbor interaction model for graphene of the type

$$\mathscr{H} = -t \sum_{\langle mn\rangle\sigma} \Psi^\dagger_{m\sigma} \sigma^x \Psi_{n\sigma} + \sum_{m\sigma} \Psi^\dagger_{m\sigma} \mathbf{U}(\mathbf{r}_m) \Psi_{m\sigma}, \quad (3)$$

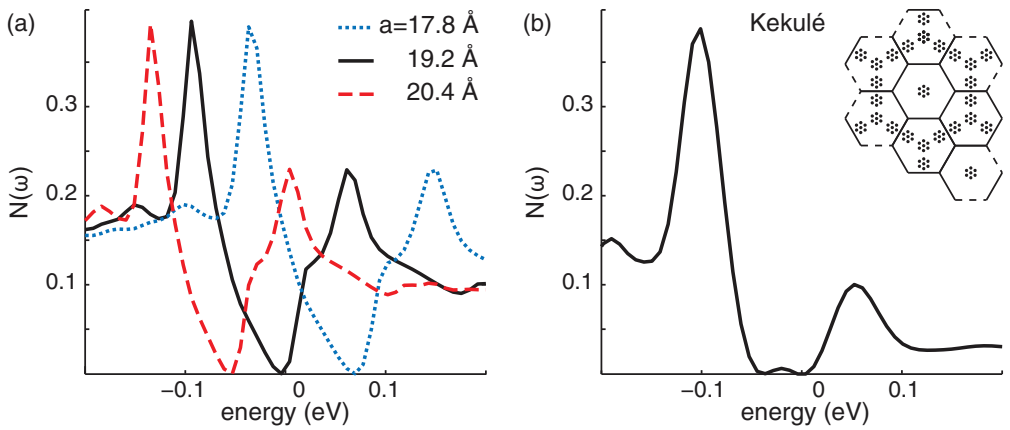

FIG. 2. (Color online) Electron DOS for (a) varying lattice parameter a, going from hole-doped (dotted line) via nearly neutral (solid line) to electron-doped (dashed line) molecular graphene, and (b) Kekulé texturing of the scattering centers. The inset shows the geometry of the Kekulé texturing. Other parameters are as in Fig. 1.

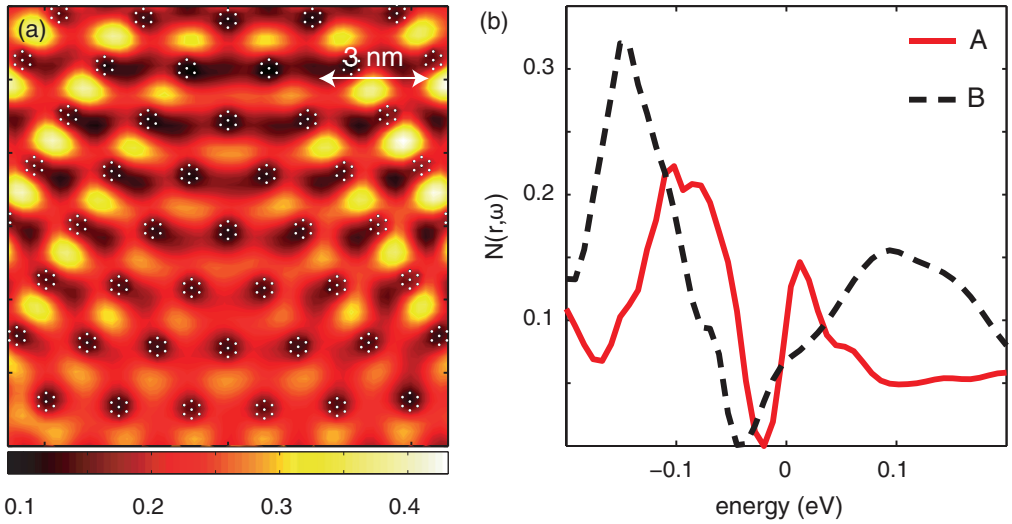

FIG. 3. (Color online) Molecular graphene under a pseudomagnetic field corresponding to 60 T ($q = 10^{-3}$ Å). (a) Spectral density and (b) electron DOS in the A (solid line) and B (dashed line) sublattices.

where $\Psi^{\dagger}_{m\sigma} = (a^{\dagger}_{m\sigma}\ b^{\dagger}_{m\sigma})$ denotes the pseudospinor for creation of electrons in the A and B sublattices, respectively, t is the hopping parameter, and σ^x is the x component of the Pauli matrices. In the last term $\mathbf{U}(\mathbf{r}_m) = \mathrm{diag}\{U_A(\mathbf{r}_m)\ U_B(\mathbf{r}_m)\}$ is a diagonal matrix representing the scattering potential and its coupling to the A and B sublattices, respectively. In this form we can describe scattering from a single vacancy in graphene by letting, for example, $\mathbf{U}(\mathbf{R}_0) = \mathrm{diag}\{U_A(\mathbf{R}_0)\ 0\}$, where $\mathbf{R}_0$ is a C site in the A sublattice. This describes scattering off a potential U_A in the A sublattice but none in the B sublattice.

Calculating the resulting electronic structure due to this potential scattering through, for example, a T-matrix approach (see Refs. 37–39 for more details), one can write the real-space local electron DOS in the B sublattice as $N_B(\mathbf{r},\omega) = \omega N_0 + \delta N_B(\mathbf{r},\omega)$, where

$$\delta N_B(\mathbf{r},\omega) = -N_0 J_0^2(k_F|\mathbf{r}-\mathbf{R}_0|)\mathrm{Im}\frac{(2D+i\pi)^2}{U_A^{-1} - \omega[2\ln(D/|\omega|)+i\pi]}. \quad (4)$$

Here, N_0 is related to the Fermi velocity v_F and a high-energy cutoff $D \sim 5$–10 eV,[37] k_F is the Fermi wave vector, and $J_0(x)$ is a Bessel function of the first kind. The correction $\delta N_B(\mathbf{r},\omega)$ displays clear divergent characteristics for $2\omega\ln(D/|\omega|) \to 1/U_A$ in a spatial neighborhood around the vacancy. Hence, the potential scattering creates a resonance within the linear part of the spectrum for large scattering potentials U_A. This feature is tightly associated with the density in the B sublattice, which can be seen since the corresponding electron DOS in the A sublattice acquires the form $N_A(\mathbf{r},\omega) = N_0\omega[1 + J_0^2(k_F|\mathbf{r} - \mathbf{R}_0|)]$ (for large U_A). It is clear that the modified density in the A sublattice lacks the divergent component. A threefold spatial symmetry is therefore expected to emerge for the electron density around the vacancy.

In molecular graphene, the vacancy defect is realized by adding a scattering center, henceforth referred to as the *vacancy site*, at a point corresponding to a C site in, say, the A sublattice [see inset of Fig. 4(b)]. The vacancy site breaks the *bond* between this C site and the adjacent C sites in the B sublattice, which locally depletes the electron density at this site, in agreement with the expected features around a vacancy site. In Fig. 4(a) we plot the local electron DOS in the lattice sites adjacent to the vacancy site for increasing potential strength. The potential strength is modulated by varying the number of scattering points in the vacancy site. The plots illustrate how the resonance builds up within the linear part of the spectrum for an increasing number of scattering points in the vacancy site, in agreement with Eq. (4), from a minor hump for the weakest scattering potential (solid line) to a more pronounced shoulder (dashed, dash-dotted, and dotted lines) for the stronger ones. By dividing out the unperturbed electron DOS [Fig. 4(a), thin line] from the perturbed ones, those features become more apparent [see Fig. 4(b)]. The plots illustrate the rise of a rather sharp resonance for the strong scattering potentials. Also the topography around the scattering potential is modulated by the increased potential strength [see Figs. 4(c) and 4(d), which show the spectral density for 7 and 13 scattering points within the vacancy site, respectively]. As expected, the vacancy scattering generates a threefold symmetric spatial signature in the B sublattice, as well as an increased electron density with increasing potential strength. The emergence of the resonance within the linear part of the spectrum, sometimes referred to as a midgap state, is caused by breaking the sublattice symmetry. The relatively weak resonance obtained in our computations compared to the prediction made in terms of Eq. (4) is reasonable since our finite lattice does not generate the very strong electronic confinement acquired in a proper two-dimensional structure. Moreover, the effective potential at the vacancy site is most likely still in the weak limit, even in the case of 37 scattering points in the vacancy site. Our computations, nevertheless, demonstrate the correct tendency of the resulting electronic density around the vacancy.

Scattering off an impurity at a plaquette position (inside a hexagon) can be accounted for by removing one of the scattering sites in the triangular lattice, hence allowing

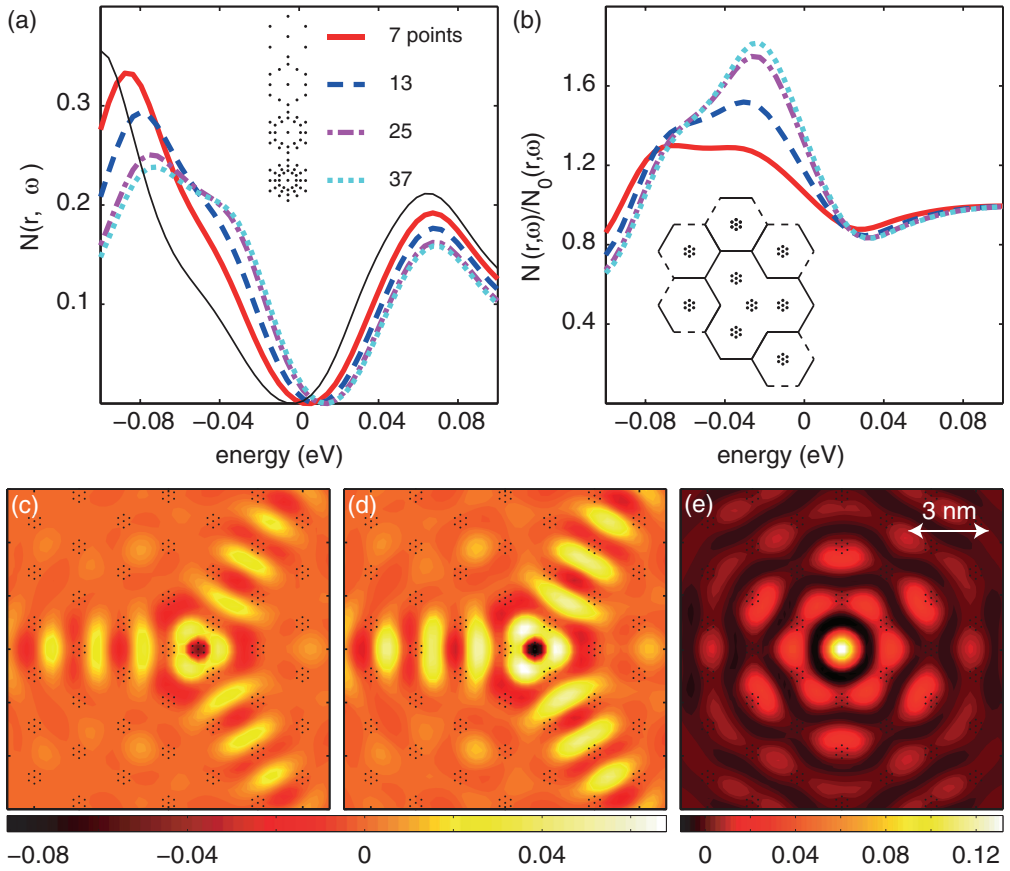

FIG. 4. (Color online) Effect of a single defect in molecular graphene. (a) Electron DOS for a varying number {7,13, 25, 37} of scattering points within the *vacancy* site. The thin line shows the unperturbed electron DOS for reference. (b) Perturbed divided by unperturbed electron DOS. The inset shows the geometry of the modified lattice including the vacancy site. The spatial spectral density for the cases of (c) 7 and (d) 13 scattering points at the vacancy site. (e) Spatial spectral density for a single impurity in the plaquette position.

electron density to fill the void and create a bond across the hexagon through the impurity [see the spectral density plotted in Fig. 4(e)]. The bright spot signifies the increased electron density at the impurity site, and the associated sixfold symmetry of the spatial signature surrounding it is apparent. In this case a resonance builds up in both sublattices for strong enough scattering potential since the impurity couples equally strongly to both.

IV. SUMMARY

In summary, we have studied molecular graphene using a scattering theoretical approach. Molecular graphene is constructed from the redistribution of the electron density constrained by a triangular lattice of scattering centers, dual to the honeycomb lattice. Making use of pointlike scattering potentials, we find that scattering centers comprising several (about seven) scattering points distributed in a hexagonal shape with a diameter between roughly 3 and 6 Å are sufficient to obtain a V-shaped spectrum. This shows that spatially continuous scattering potentials are not necessary to achieve realistic electronic structures. Combining those scattering centers with a moderately sized finite lattice (∼13 × 14 scattering centers), we reproduce results in very good agreement with Ref. 11.

Impurity scattering can be realized by adding or removing scattering centers in the system. An important finding is that we verify that local defects may give rise to sharp resonances within the V-shaped DOS, provided that the scattering potential is sufficiently strong. This is in good agreement with previous theoretical predictions.[37–39] Our results suggest that defects of the same species as the surrounding lattice comprise a scattering potential which is not sufficiently strong to generate a resonance in the local DOS, which we believe to be the cause of the lack of experimental confirmation of this feature. Entities that correspond to stronger scattering potentials which thereby deplete the electron density more efficiently than the surrounding lattice should be accessible to the present experimental state of the art. Thus, experimental verification of the theoretical prediction should be within the realms of experiments in the near future.

ACKNOWLEDGMENTS

We thank A. V. Balatsky and O. Eriksson for useful conversations. Support from the Swedish Research Council is acknowledged.

*Jonas.Fransson@physics.uu.se

[1] K. S. Novoselov, A. K. Geim, S. V. Morozov, D. Jiang, Y. Zhang, S. V. Dubonos, I. V. Grigorieva, and A. A. Firsov, Science **306**, 666 (2004).

[2] A. K. Geim and K. S. Novoselov, Nat. Mater. **6**, 183 (2007).

[3] M. I. Katsnelson, Mater. Today **10**, 20 (2007).

[4] A. H. Castro Neto, F. Guinea, N. M. R. Peres, K. S. Novoselov, and A. K. Geim, Rev. Mod. Phys. **81**, 109 (2009).

[5] M. A. H. Vozmediano, M. I. Katsnelson, and F. Guinea, Phys. Rep. **496**, 109 (2010).

[6] D. C. Elias, R. R. Nair, T. M. G. Mohiuddin, S. V. Morozov, P. Blake, M. P. Halsall, A. C. Ferrari, D. W. Boukhvalov, M. I. Katsnelson, A. K. Geim, and K. S. Novoselov, Science **323**, 610 (2009).

[7] M. Polini, F. Guinea, M. Lewenstein, H. C. Manoharan, and V. Pellegrini, Nat. Nanotechnol. **8**, 625 (2013).

[8] O. Peleg, G. Bartal, B. Freedman, O. Manela, M. Segev, and D. N. Christodoulides, Phys. Rev. Lett. **98**, 103901 (2007).

[9] U. Kuhl, S. Barkhofen, T. Tudorovskiy, H.-J. Stöckmann, T. Hossain, L. de Forges de Parny, and F. Mortessagne, Phys. Rev. B **82**, 094308 (2010).

[10] A. Singha, M. Gibertini, B. Karmakar, S. Yuan, M. Polini, G. Vignale, M. I. Katsnelson, A. Pinczuk, L. N. Pfeiffer, K. W. West, and V. Pellegrini, Science **332**, 1176 (2011).

[11] K. K. Gomes, W. Mar, W. Ko, F. Guinea, and H. C. Manoharan, Nature (London) **483**, 306 (2012).

[12] P. Soltan-Panahi, J. Struck, P. Hauke, A. Bick, W. Plenkers, G. Meineke, C. Becker, P. Windpassinger, M. Lewenstein, and K. Sengstock, Nat. Phys. **7**, 434 (2011).

[13] L. Tarruell, D. Greif, T. Uehlinger, G. Jotzu, and T. Esslinger, Nature (London) **483**, 302 (2012).

[14] T. Uehlinger, G. Jotzu, M. Messer, D. Greif, W. Hofstetter, U. Bissbort, and T. Esslinger, Phys. Rev. Lett. **111**, 185307 (2013).

[15] F. D. M. Haldane, Phys. Rev. Lett. **61**, 2015 (1988).

[16] C. L. Kane and E. J. Mele, Phys. Rev. Lett. **95**, 226801 (2005).

[17] F. Guinea, M. I. Katsnelson, and A. K. Geim, Nat. Phys. **6**, 30 (2010).

[18] Z. Y. Meng, T. C. Lang, S. Wessel, F. F. Assaad, and A. Muramatsu, Nature (London) **464**, 847 (2010).

[19] G. A. Fiete and E. J. Heller, Rev. Mod. Phys. **75**, 933 (2003).

[20] B. Wunsch, F. Guinea, and F. Sols, New J. Phys. **10**, 103027 (2008).

[21] C.-H. Park and S. G. Louie, Nano. Lett. **9**, 1793 (2009).

[22] M. Gibertini, A. Singha, V. Pellegrini, M. Polini, G. Vignale, A. Pinczuk, L. N. Pfeiffer, and K. W. West, Phys. Rev. B **79**, 241406 (2009).

[23] J. Fransson, H. C. Manoharan, and A. V. Balatsky, Nano Lett. **10**, 1600 (2010).

[24] H. Gawronski, J. Fransson, and K. Morgenstern, Nano Lett. **11**, 2720 (2011).

[25] J.-H. She, J. Fransson, A. R. Bishop, and A. V. Balatsky, Phys. Rev. Lett. **110**, 026802 (2013).

[26] J. Fransson, J.-H. She, L. Pietronero, and A. V. Balatsky, Phys. Rev. B **87**, 245404 (2013).

[27] C. F. Hirjibehedin, C. P. Lutz, and A. J. Heinrich, Science **312**, 1021 (2006).

[28] L. Zhou, J. Wiebe, S. Lounis, E. Vedmedenko, F. Meier, S. Blügel, P. H. Dederichs, and R. Wiesendanger, Nat. Phys. **6**, 187 (2010).

[29] R. Decker, Y. Wang, V. W. Brar, W. Regan, H.-Z. Tsai, Q. Wu, W. Gannett, A. Zettl, and M. F. Crommie, Nano Lett. **11**, 2291 (2011).

[30] Y. Wang, V. W. Brar, A. V. Shytov, Q. Wu, W. Regan, H.-Z. Tsai, A. Zettl, L. S. Levitov, and M. F. Crommie, Nat. Phys. **8**, 653 (2012).

[31] S. Loth, S. Baumann, C. P. Lutz, D. M. Eigler, and A. J. Heinrich, Science **335**, 196 (2012).

[32] A. A. Khajetoorians, J. Wiebe, B. Chilian, and R. Wiesendanger, Science **332**, 1062 (2011).

[33] C. R. Moon, L. S. Mattos, B. K. Foster, G. Zeltzer, W. Ko, and H. C. Manoharan, Science **319**, 782 (2008).

[34] G. Binnig, H. Rohrer, Ch. Gerber, and E. Weibel, Appl. Phys. Lett. **40**, 178 (1982).

[35] J. Tersoff and D. R. Hamann, Phys. Rev. Lett. **50**, 1998 (1983).

[36] J. Fransson and A. V. Balatsky, Phys. Rev. B **85**, 161401(R) (2012).

[37] S. H. M. Jafri, K. Carva, E. Widenkvist, T. Blom, B. Sanyal, J. Fransson, O. Eriksson, U. Jansson, H. Grennberg, O. Karis, R. A. Quinlan, B. C. Holloway, and K. Leifer, J. Phys. D **43**, 045404 (2010).

[38] K. Carva, B. Sanyal, J. Fransson, and O. Eriksson, Phys. Rev. B **81**, 245405 (2010).

[39] T. O. Wehling, A. V. Balatsky, M. I. Katsnelson, A. I. Lichtenstein, K. Scharnberg, and R. Wiesendanger, Phys. Rev. B **75**, 125425 (2007).